Measurement of Quadratic Terahertz Optical Nonlinearities Using Second-Harmonic Lock-in Detection

Shuai Lin, Shukai Yu, and Diyar Talbayev*

Department of Physics and Engineering Physics, Tulane University, 6400 Freret Street, New Orleans, Louisiana 70118, USA

(Received 7 June 2018; revised manuscript received 12 August 2018; published 2 October 2018)

We present a method to measure quadratic terahertz optical nonlinearities in terahertz time-domain spectroscopy. We use a rotating linear polarizer (a polarizing chopper) to modulate the amplitude of the incident terahertz pulse train. We use phase-sensitive lock-in detection at the fundamental and the second harmonic of the modulation frequency to separate the materials' responses that are linear and quadratic in a terahertz electric field. We demonstrate this method by measuring the quadratic terahertz Kerr effect in the presence of the much stronger linear electro-optic effect in the (110) GaP crystal. We propose that the method can be used to detect terahertz second-harmonic generation in noncentrosymmetric media in time-domain spectroscopy, with broad potential applications in nonlinear terahertz photonics and related technology.

DOI: 10.1103/PhysRevApplied.10.044007

I. INTRODUCTION

Nonlinear terahertz optics has blossomed into an exciting and active area of research with the advent of tabletop high-field terahertz sources [1–5]. Among a multitude of nonlinear phenomena, we focus here on the nonlinearities that are quadratic in a terahertz electric field E^T. Such quadratic effects can be induced in the second and third orders via the nonlinear polarizabilities $\chi^{(2)}(E^T)^2$ and $\chi^{(3)}(E^T)^2E^\omega$, where E^ω is an optical field. The second-order nonlinearity $\chi^{(2)}$ can lead to second-harmonic generation (or sum-frequency mixing) in noncentrosymmetric crystals. While it appears that the peak electric field strength available from tabletop terahertz sources may be sufficient to generate the second harmonic of the fundamental terahertz pulse [6], terahertz second-harmonic generation has not yet been reported. For a typical time-domain single-cycle fundamental terahertz pulse, the second-harmonic terahertz pulse generated will have a significant time-domain and spectral overlap with the fundamental terahertz pulse. This makes it difficult to distinguish the fundamental and second-harmonic terahertz waves in a measurement, as the second-harmonic amplitude may be several orders of magnitude smaller than the fundamental amplitude [6].

The third-order nonlinearity $\chi^{(3)}$ results in a terahertz-induced optical birefringence proportional to $(E^T)^2$, also termed the "terahertz Kerr effect." The birefringence can be detected as polarization rotation of the optical gating beam E^ω in a measurement. The first observation of the terahertz Kerr effect was reported by Hoffmann *et al.* [7] in several liquids. Following their observation, the terahertz Kerr effect was investigated in many other liquid and solid materials [8–17]. Up to now, the reported observations of the terahertz Kerr effect occurred in liquids or crystals in geometries where the quadratic terahertz-induced birefringence is not obscured by the linear electro-optic (Pockels) effect. The latter effect results from the second-order nonlinearity and provides a common means for time-domain detection of a terahertz electric field with use of femtosecond optical pulses—electro-optic sampling [18–20]. When both electro-optic effects are present, the linear birefringence due to the Pockels effect is usually much stronger than the quadratic birefringence due to the terahertz Kerr effect. Measuring and characterizing the much-weaker terahertz Kerr effect in the presence of the stronger Pockels effect is a difficult experimental task.

In this article, we present a method to measure quadratic terahertz optical nonlinearities that scale as $(E^T)^2$. We illustrate the method by measuring the terahertz Kerr effect in a (110)-oriented GaP crystal via the optical birefringence due to the third-order nonlinear polarizability $\chi^{(3)}(E^T)^2E^\omega$, where E^ω is the electric field of the optical gating beam. Importantly, the (110)-oriented GaP crystal also exhibits a much stronger birefringence due to the linear electro-optic Pockels effect governed by the second-order polarizability $\chi^{(2)}E^TE^\omega$. We show that our method allows the separation and reliable measurement of the two effects, one of which is quadratic and the other is linear in the terahertz field E^T. We also show how this method can be extended to the time-domain detection of the terahertz second-harmonic generation due to the second-order

*dtalbaye@tulane.edu

polarization of the form $\chi^{(2)}(E^T)^2$. Our method shows a strong potential for broad adoption and application in nonlinear terahertz photonics.

II. EXPERIMENTAL RESULTS AND DISCUSSION

Our measurement uses a terahertz time-domain spectrometer based on a regenerative amplifier with a repetition rate of 1-kHz. We use optical rectification and tilted-wavefront phase matching in a $LiNbO_3$ prism to generate high-field terahertz pulses. We use linear electro-optic sampling in a (110)-oriented GaP crystal for terahertz detection [18–20] and estimate that the peak electric field incident on GaP is more than 100 kV/cm [21]. The 1-kHz train of vertically polarized terahertz pulses from $LiNbO_3$ is modulated by a continuously rotating wire-grid polarizer—the polarizing chopper [22,23]. The terahertz pulse train then passes through a fixed wire-grid polarizer with a horizontal transmission axis [Fig. 1(a)]. This arrangement results in a sinusoidal modulation of the terahertz pulse train in which the polarity of the terahertz pulse switches from positive to negative [Fig. 1(b)]. The sinusoidal modulation frequency f is 77 Hz. The terahertz field incident on the (110)-oriented-GaP receiver is horizontally polarized and the gating optical beam is vertically polarized. The time-domain amplitude of the terahertz pulse is measured with balanced photodiodes and a lock-in amplifier with f as the reference frequency [Fig. 1(a)]. The measured quantity $\Delta I(t)$ is the difference in the gating-beam intensity on the balanced photodiodes as a function of the time t between the gating optical pulse and the terahertz field. $\Delta I(t)$ is proportional to the linear terahertz-induced birefringence due to the electro-optic Pockels effect [18–20]. This method is commonly known as "electro-optic sampling." Figure 2(a) shows the measured terahertz-field pulses in the time domain.

The same setup also allows the measurement of the terahertz Kerr effect that scales as $(E^T)^2$. The product $(E^T)^2$ is modulated by the polarizing chopper at twice the fundamental frequency, $2f$, as illustrated in Fig. 1(c). By detecting the quantity $\Delta I(t)$ at the second harmonic of the fundamental modulation frequency ($2f = 154$ Hz), we measure the terahertz Kerr effect in (110) GaP. Figure 2(b) displays the time-domain $(E^T)^2$ spectra measured this way. The colors of the terahertz Kerr spectra in Fig. 2(b) correspond to the same-color linear terahertz spectra in Fig. 2(a). We emphasize that the measurements reported in Figs. 2(a) and 2(b) are taken under the same experimental conditions and geometry. The only difference between the measurements is the lock-in-amplifier detection at the fundamental and the second-harmonic frequency of the polarizing-chopper modulation. The terahertz amplitude in Fig. 2(a) is varied by insertion of high-resistivity Si wafers in the path of the terahertz beam; the number of wafers ranges from 0 to 3. Figure 2(c) quantifies the peak

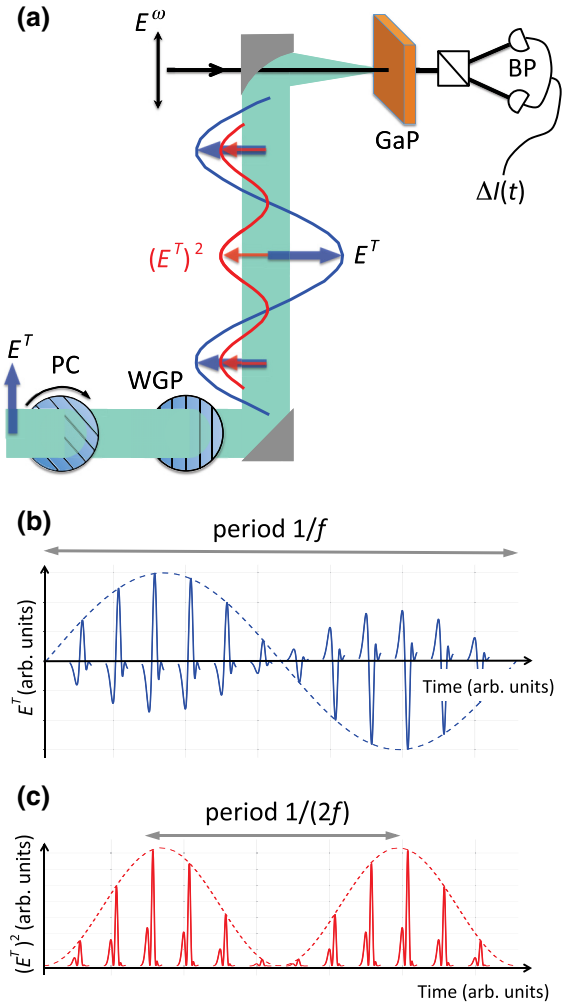

FIG. 1. (a) The second-harmonic lock-in detection experiment. The $LiNbO_3$ source of terahertz pulses E^T is not shown. A 1-kHz train of vertically polarized terahertz pulses passes through the polarizing chopper (PC) and a fixed wire-grid polarizer (WGP) with a horizontal transmission axis. After the WGP, the terahertz pulse train is horizontally polarized and sinusoidally modulated at frequency f (the blue sinusoid). The product $(E^T)^2$ is modulated at frequency $2f$ (the red sinusoid). The terahertz pulse train impinges on the (110)-oriented GaP receiver for detection by the vertically polarized gating beam E^ω. Balanced photodiodes (BP) measure the terahertz-induced birefringence in GaP. (b) The sinusoidally modulated terahertz pulse train after the WGP. The polarization is horizontal and the strength of the terahertz electric field changes sinusoidally over one period. The terahertz pulses change polarity from positive to negative. The duration of the terahertz pulses and the pulse separation are not drawn to scale. (c) Sinusoidal modulation of the product $(E^T)^2$. The modulation frequency is $2f$.

amplitude of $(E^T)^2$ as a function of the peak amplitude of E^T; the highest peak amplitude of each quantity is normalized to 1 in Fig. 2(c). As expected, we observe that the relationship is quadratic. The second-harmonic lock-in

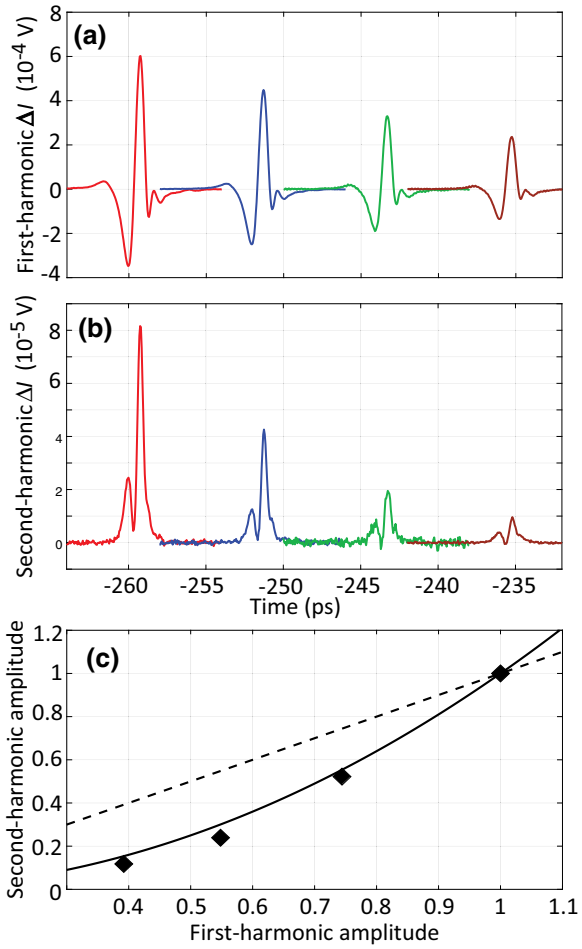

FIG. 2. (a) Time-domain terahertz pulses E^T measured by linear electro-optic sampling and first-harmonic detection. The pulses of different amplitude are obtained by insertion of high-resistivity Si wafers in the path of the terahertz beam. The number of wafers ranges from 0 to 3. (b) Time-domain $(E^T)^2$ spectra measured by second-harmonic lock-in detection and the quadratic electro-optic effect. The colors of the spectra correspond to the same-color spectra in (a). (c) Relative peak amplitudes of the first- and second-harmonic spectra in (a),(b). Diamonds represent measured amplitudes, the dashed line is a linear function, and the solid line is a quadratic function.

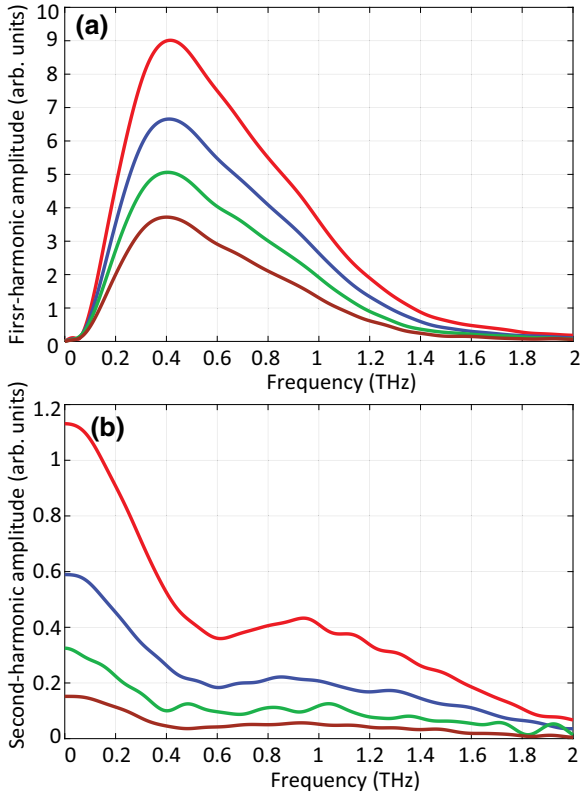

FIG. 3. (a) Frequency-domain amplitudes for the first-harmonic time-domain spectra in Fig. 2(a). (b) Frequency-domain amplitudes for the second-harmonic time-domain spectra in Fig. 2(b).

detection allows us to directly measure the quadratic terahertz Kerr birefringence in the presence of linear electro-optic Pockels birefringence that is more than 20 times stronger.

Figure 3 compares the frequency content of the linear and quadratic terahertz spectra measured via first- and second-harmonic lock-in detection. The frequency-domain spectra in Fig. 3 display the Fourier-transform amplitude of the spectra in Figs. 2(a) and 2(b). Figure 3(a) shows typical linear frequency-domain terahertz spectra with near-identical frequency content for the different terahertz peak amplitudes incident on the GaP receiver. The linear frequency-domain spectra peak just above 0.4 THz. The quadratic, second-harmonic terahertz spectra peak around 0.8–0.9 THz, twice the frequency of the linear-spectrum frequency peak. The second-harmonic spectra also possess a large zero-frequency component because $(E^T)^2$ in the time domain has no negative components. For comparison, we compute $(E^T)^2$ and its Fourier transform from the measured linear E^T. In these numerically computed spectra, the zero-frequency component always has twice the amplitude of the high-frequency peak. The experimentally measured $(E^T)^2$ spectra follow this trend only roughly [Fig. 3(b)].

The data presented in Figs. 2 and 3 provide strong evidence that the second-harmonic lock-in detection measures the quadratic terahertz nonlinearity due to the terahertz Kerr effect. The induced terahertz Kerr birefringence is described by the third-order nonlinear polarization

$$P_i^{(3)} = \chi_{ijkl}^{(3)} E_j^T E_k^T E_l^{\omega}, \tag{1}$$

where the Cartesian coordinates $i,j,k,l = 1$, 2, or 3 and a summation over repeated indices is implied. The third-order nonlinear tensor $\chi_{ijkl}^{(3)}$ has 21 nonzero elements, of

which four are independent [24]:

$$\begin{aligned} xxxx &= yyyy = zzzz, \\ yyzz &= zzyy = zzxx = xxzz = xxyy = yyxx, \\ yzyz &= zyzy = zxzx = xzxz = xyxy = yxyx, \\ yzzy &= zyyz = zxxz = xzzx = xyyx = yxxy. \end{aligned} \tag{2}$$

Equations (1) and (2) allow the modeling of terahertz Kerr birefringence as a function of the angular orientation of the (110) GaP crystal. For a complete model of such angular dependence, knowledge of the four independent nonlinear parameters in Eq. (2) is necessary. In the absence of such knowledge, we can compute the terahertz Kerr birefringence and the balanced photodiode current $\Delta I(t)$ for the two special cases $\alpha = 0^\circ$ and $\alpha = 90^\circ$. We define α as the angle between the peak terahertz electric field vector and the in-plane [001] direction of the GaP crystal. We use the Cartesian-coordinate system associated with the GaP crystal and shown in Fig. 4. The x, y, and z axes correspond to the cubic [100], [010], and [001] directions in this system.

In the case $\alpha = 0^\circ$, we set

$$\vec{E}^T = E_0^T \begin{pmatrix} 0 \\ 0 \\ 1 \end{pmatrix} \quad \text{and} \quad \vec{E}^\omega = \frac{E_0^\omega}{\sqrt{2}} \begin{pmatrix} -1 \\ 1 \\ 0 \end{pmatrix}$$

and obtain

$$\vec{P}^{(3)} = \begin{pmatrix} \chi^{(3)}_{xyyx} (E_0^T)^2 E_x^\omega \\ \chi^{(3)}_{xyyx} (E_0^T)^2 E_y^\omega \\ 0 \end{pmatrix}.$$

Under these conditions, the new principal axes of the refractive index ellipsoid correspond to the directions [110], [$\bar{1}$10], and [001], which we label as x', y', and z'. The

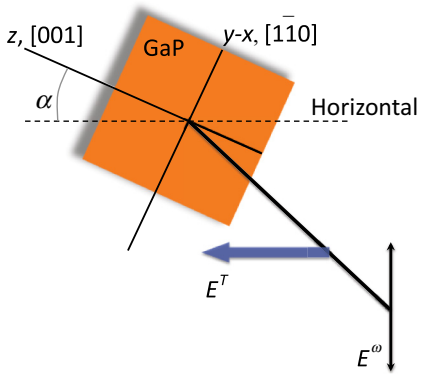

FIG. 4. Geometry of the linear electro-optic and terahertz Kerr birefringence measurements on the (110)-oriented GaP crystal. The peak terahertz electric field E^T is horizontal. The optical gating beam E^ω is polarized vertically. α labels the angle between the [001] z axis of the crystal and the horizontal. The other crystalline axes are [100] x and [010] y.

third-order polarization in these new coordinates becomes

$$\vec{P}'^{(3)} = \begin{pmatrix} 0 \\ \chi^{(3)}_{xyyx} (E_0^T)^2 E_{y'}^\omega \\ 0 \end{pmatrix}.$$

The gating beam E^ω is polarized along the principal y' axis and does not experience polarization rotation due to the terahertz Kerr effect. Thus, $\Delta I(t) = 0$ for $\alpha = 0^\circ$. In the case $\alpha = 90^\circ$, we set

$$\vec{E}^T = \frac{E_0^T}{\sqrt{2}} \begin{pmatrix} 1 \\ -1 \\ 0 \end{pmatrix} \quad \text{and} \quad \vec{E}^\omega = E_0^\omega \begin{pmatrix} 0 \\ 0 \\ 1 \end{pmatrix}$$

and obtain

$$\vec{P}^{(3)} = \begin{pmatrix} 0 \\ 0 \\ \chi^{(3)}_{xyyx} (E_0^T)^2 E_z^\omega \end{pmatrix}.$$

The [001] z direction remains a principal axis of the refractive-index ellipsoid, and the gating beam remains polarized along z. Thus, $\Delta I(t) = 0$ for $\alpha = 90^\circ$.

Our measurements confirm that $\Delta I(t) = 0$ for $\alpha = 0^\circ$ and 90° when detected at the second harmonic, corresponding to the terahertz Kerr effect. When detected at the first harmonic, $\Delta I(t)$ is zero for $\alpha = 0^\circ$, but for $\alpha = 90^\circ$ it exhibits a maximum, which is the position of the most efficient linear electro-optic detection of the terahertz waveform [25]. The data presented in Figs. 2 and 3 are collected near the angle $\alpha = 70^\circ$, close to the maximum of first-harmonic balanced photodiode signal $\Delta I(t)$.

We now show that second-harmonic lock-in detection can be used to measure terahertz second-harmonic generation in noncentrosymmetric media due to the second-order polarizability $P_i^{(2)} = \chi_{ijk}^{(2)} E_j^T E_k^T$. In this measurement, the terahertz pulses are focused into a sample, generating the terahertz second harmonic after passing through the fixed wire-grid polarizer, Fig. 1. The second-harmonic terahertz pulse $E^{T(2)}$ generated propagates together with the fundamental terahertz pulse E^T after passing through the sample. This propagating terahertz wave $E^{T(2)}$ can be detected via the linear electro-optic effect in the GaP receiver. In a conventional terahertz time-domain spectrometer without the polarizing chopper and sinusoidal modulation, it is difficult to separate the contributions of $E^{T(2)}$ and E^T to the linear electro-optic effect, since the two pulses copropagate with significant overlap in both the time domain and the frequency domain. In addition, the expected amplitude of the second-harmonic pulse $E^{T(2)}$ generated may be several orders of magnitude smaller than the fundamental amplitude E^T [6]. The sinusoidal modulation by the polarizing chopper allows the separation of the two waves, as the second-harmonic wave $E^{T(2)}$ is modulated at twice the sinusoidal modulation frequency [Fig. 1].

Then the fundamental terahertz wave E^T is detected at the fundamental modulation frequency and the second-harmonic wave $E^{T(2)}$ is measured by the lock-in amplifier at the second harmonic of the sinusoidal modulation frequency. We emphasize that both waves are measured via the linear electro-optic Pockels effect in GaP, but are separated via the first- and second-harmonic lock-in detection. To distinguish the linear electro-optic effect due to $E^{T(2)}$ and the quadratic terahertz Kerr effect due to E^T in the GaP receiver, which are both measured in the second-harmonic lock-in detection, we must eliminate the latter by choosing the angle $\alpha = 90^\circ$ in the configuration in Fig. 4. In this geometry, the terahertz Kerr effect is zero and the electro-optic Pockels effect is maximized [25]. This scheme should allow the measurement of terahertz second-harmonic generation that so far has eluded researchers. Theoretical studies of possible materials for observing the phenomenon have been rare. Merbold *et al.* [6] considered the use of metal nanoslits and split-ring resonators to enhance the peak terahertz field and the nonlinear interactions. They predict that terahertz second-harmonic generation could potentially be observed in $LiTaO_3$ with the help of terahertz-field enhancement by the nanoslits or the split-ring resonators.

III. CONCLUSIONS

In summary, we present a measurement of the quadratic terahertz Kerr effect in the (110)-oriented zinc-blende crystal GaP. In our measurement geometry, the terahertz Kerr birefringence is superimposed on the much-stronger birefringence due to the linear electro-optic effect. We use sinusoidal terahertz-pulse-train modulation and second-harmonic lock-in detection to separate and measure the much-weaker terahertz Kerr birefringence. More generally, our measurement method allows the separation of the electro-optic signals proportional to E^T and $(E^T)^2$, as evidenced by the data presented. We predict that our method will allow the measurement of the elusive terahertz second-harmonic generation in noncentrosymmetric media, which opens a new area of exploration in nonlinear optics and optical properties of materials—second-harmonic terahertz spectroscopy and related photonic technologies.

ACKNOWLEDGMENTS

The work at Tulane University was supported by the the NSF (Grant No. DMR-1554866) and the Carol Lavin Bernick Faculty Grant Program.

[1] J. Hebling, K.-L. Yeh, M. C. Hoffmann, B. Bartal, and K. A. Nelson, Generation of high-power terahertz pulses by tilted-pulse-front excitation and their application possibilities, J. Opt. Soc. Am. B **25**, B6 (2008).

[2] M. C. Hoffmann, J. Hebling, H. Y. Hwang, K.-L. Yeh, and K. A. Nelson, THz-pump/THz-probe spectroscopy of semiconductors at high field strengths, J. Opt. Soc. Am. B **26**, A29 (2009).

[3] H. Hirori, A. Doi, F. Blanchard, and K. Tanaka, Single-cycle terahertz pulses with amplitudes exceeding 1 MV/cm generated by optical rectification in $LiNbO_3$, Appl. Phys. Lett. **98**, 091106 (2011).

[4] H. Y. Hwang, S. Fleischer, N. C. Brandt, B. G. Perkins Jr, M. Liu, K. Fan, A. Sternbach, X. Zhang, R. D. Averitt, and K. A. Nelson, A review of non-linear terahertz spectroscopy with ultrashort tabletop-laser pulses, J. Mod. Opt. **62**, 1447 (2015).

[5] T. Kampfrath, K. Tanaka, and K. Nelson, Resonant and nonresonant control over matter and light by intense terahertz transients, Nature Photon. **7**, 680 (2013).

[6] H. Merbold, A. Bitzer, and T. Feurer, Second harmonic generation based on strong field enhancement in nanostructured THz materials, Opt. Express **19**, 7262 (2011).

[7] M. C. Hoffmann, N. C. Brandt, H. Y. Hwang, K.-L. Yeh, and K. A. Nelson, Terahertz Kerr effect, Appl. Phys. Lett. **95**, 231105 (2009).

[8] M. Zalkovskij, A. C. Strikwerda, K. Iwaszczuk, A. Popescu, D. Savastru, R. Malureanu, A. V. Lavrinenko, and P. U. Jepsen, Terahertz-induced Kerr effect in amorphous chalcogenide glasses, Appl. Phys. Lett. **103**, 221102 (2013).

[9] M. Cornet, J. Degert, E. Abraham, and E. Freysz, Terahertz Kerr effect in gallium phosphide crystal, J. Opt. Soc. Am. B **31**, 1648 (2014).

[10] M. A. Allodi, I. A. Finneran, and G. A. Blake, Nonlinear terahertz coherent excitation of vibrational modes of liquids, J. Chem. Phys. **143**, 234204 (2015).

[11] M. Sajadi, M. Wolf, and T. Kampfrath, Terahertz-field-induced optical birefringence in common window and substrate materials, Opt. Express **23**, 28985 (2015).

[12] S. Sarbak, G. Sharma, C. S. Joseph, W. E. Kucia, K. Dobek, R. H. Giles, and A. Dobek, Direct observation of the THz Kerr effect (TKE) in deionized, distilled and buffered (PBS) water, Phys. Chem. Chem. Phys. **19**, 26749 (2017).

[13] M. Shalaby, C. Vicario, and C. P. Hauri, Extreme nonlinear terahertz electro-optics in diamond for ultrafast pulse switching, APL Photonics **2**, 036106 (2017).

[14] S. Bodrov, Y. Sergeev, A. Murzanev, and A. Stepanov, Terahertz induced optical birefringence in polar and nonpolar liquids, J. Chem. Phys. **147**, 084507 (2017).

[15] M. Sajadi, M. Wolf, and T. Kampfrath, Transient birefringence of liquids induced by terahertz electric-field torque on permanent molecular dipoles, Nat. Commun. **8**, 14963 (2017).

[16] T. Kampfrath, M. Wolf, and M. Sajadi, The sign of the polarizability anisotropy of polar molecules is obtained from the terahertz Kerr effect, Chem. Phys. Lett. **692**, 319 (2018).

[17] T. Kampfrath, R. K. Campen, M. Wolf, and M. Sajadi, The nature of the dielectric response of methanol revealed by the terahertz Kerr effect, J. Phys. Chem. Lett. **9**, 1279 (2018).

[18] Q. Wu, M. Litz, and X. Zhang, Broadband detection capability of ZnTe electro-optic field detectors, Appl. Phys. Lett. **68**, 2924 (1996).

[19] A. Nahata, A. S. Weling, and T. F. Heinz, A wideband coherent terahertz spectroscopy system using optical rectification and electro-optic sampling, Appl. Phys. Lett. **69**, 2321 (1996).

[20] Q. Wu and X.-C. Zhang, 7 terahertz broadband GaP electro-optic sensor, Appl. Phys. Lett. **70**, 1784 (1997).

[21] S. Yu, K. H. Heffernan, and D. Talbayev, Beyond the effective mass approximation: A predictive theory of the nonlinear optical response of conduction electrons, Phys. Rev. B **95**, 125201 (2017).

[22] D. J. Aschaffenburg, M. R. C. Williams, D. Talbayev, D. F. Santavicca, D. E. Prober, and C. A. Schmuttenmaer, Efficient measurement of broadband terahertz optical activity, Appl. Phys. Lett. **100**, 241114 (2012).

[23] C. M. Morris, R. V. Aguilar, A. V. Stier, and N. P. Armitage, Polarization modulation time-domain terahertz polarimetry, Opt. Express **20**, 12303 (2012).

[24] R. W. Boyd, *Nonlinear Optics* (Academic Press, San Diego, 2003).

[25] P. C. M. Planken, H.-K. Nienhuys, H. J. Bakker, and T. Wenckebach, Measurement and calculation of the orientation dependence of terahertz pulse detection in ZnTe, J. Opt. Soc. Am. B **18**, 313 (2001).